Journal of Energy Storage 63 (2023) 107095

Contents lists available at ScienceDirect

Journal of Energy Storage

journal homepage: www.elsevier.com/locate/est

Research papers

# Supercapacitor auto analyser: An automated data analysis software for supercapacitor characterization

Miguel H. Boratto [a,b,*], João V.M. Lima [a], George G. Malliaras [b], Carlos F.O. Graeff [a]

[a] São Paulo State University (UNESP), School of Sciences, Department of Physics, Bauru, SP 17033-360, Brazil
[b] University of Cambridge, Electrical Engineering Division, Department of Engineering, Cambridge CB30FA, UK

ARTICLE INFO

*Keywords:*
Supercapacitors
Data analysis
Key parameters
Normalization
Metrics

ABSTRACT

High-performance supercapacitors (SCs) with high power, energy, and long-life cycles, are essential for innovating wearable and portable electronics as extensively reported in literature. The Web of Science shows more than 23,000 papers published since 2018 with the topic 'Supercapacitor', number that keep growing, from 732 papers per year in 2012 to an average of 4651 papers per year since 2018. However, the establishment of performance metrics on the reported values should be achieved to reduce inconsistencies in their real performances. For that reason, we developed the Supercapacitors Auto Analyser (SCAA) program for SCs data analysis to support the community to establish performance metrics for SC devices, with standard terms, equations, and units. The SCAA generates important graphs with the SCs key properties and electrochemical performance such as capacitance, energy, power, coulombic efficiency (CE), equivalent series resistance (ESR), drop potential ($V_{drop}$), cycling stability, and time constant. These results are calculated from common data generated by potentiostat on SCs characterization such as cyclic voltammetry (CV), galvanostatic charge–discharge (GCD), and electrochemical impedance spectroscopy (EIS). With appropriate inputs, the SCAA provides as many as 50 graphs with accurate normalizations by mass, area, or volume in a few minutes. This automation of data analysis is packed in a software made available to the community in the supplementary materials and website www.scaasoftware.com.

## 1. Introduction

The increasing interest and need for portable electronics and electric cars require even more energy storage for continuous and reliable energy supply [1–3]. It has been reported that our global energy needs will roughly double by mid-century and triple by 2100 [4]. Thus, there is an ever increasing and urgent demand for vigorous development of not only clean, renewable, and sustainable alternative energies (solar, wind and tide), but also advanced, low-cost, and environmentally friendly energy conversion and storage devices [5–8]. Among energy storage systems, supercapacitors (SCs), also known as electrochemical capacitors or ultracapacitors, have been the focus of interest from part of the community because they offer hundreds of thousands of charge/discharge cycles, superior rate capability, rapid charge/discharge rate, simple principles, fast dynamics of charge propagation and low maintenance, being an intermediate device between batteries that have a high energy density, and conventional capacitors with high power density [9–12]. In this way, the development of high-performance SCs, with high values of power, energy, and long-life cycles, is essential for innovating wearable and portable electronics [13–15].

Due to the great rise in the number of researchers focused on enhancing the stored energy in SCs, as well as creating hybrid electrochemical energy storage devices (EESD), different metrics have been published. This brings discrepancies among the different testing methods and makes the comparison between different EESD challenging. As an example, many published works call energy (or power) density the energy normalized by mass, when it should be called specific energy [16]. Studies of graphene electrodes for application in SCs are presented considering the mass of the whole device, which considers the mass of the current collectors, electrolyte, separator, and active material [17]. Other studies use the specific energy values considering only the mass of the active materials [18] or do not clearly state which mass is used in their calculations [19]. Therefore, an expressive normalization parameter based on the mass/area/volume of both the active material and the whole device is required, which should be reported together to better depict the entire energy storage device in a more accurate way

* Corresponding author at: São Paulo State University (UNESP), School of Sciences, Department of Physics, Bauru, SP 17033-360, Brazil.
*E-mail address:* mhb51@cam.ac.uk (M.H. Boratto).

https://doi.org/10.1016/j.est.2023.107095
Received 25 December 2022; Received in revised form 14 February 2023; Accepted 7 March 2023

[16,20].

Among the processes researchers employ to reach useful initial insights about their devices are sample production and electrochemical characterization followed by data analysis that may take days, and the repetition process during extensive data handling and manipulation may lead to human mistakes. Unfortunately, besides the lack of normalization, some works present calculations with different equations and parameters that may give incorrect results, over or underestimating real values. From common electrical measurements (CV, GCD, and EIS) and known generated data for input into the SCAA program the researchers' job is simplified. The program was tested with many known data to verify its credibility in the outputs, which is crucial for reliable and publication-worthy results.

Moreover, agreement on the performance metrics may be of great help for the energy community, and an automated program could contribute to these questions, as well as to accelerate the electrochemical data analysis for these scientists. Much time is addressed to manage data, performing calculations, and find the proper way to show their results and understand the key parameters of their devices. In fact, most of this time could be more valuable from more 'human-activities' as readings on paper and creative thinking for future experiments, improvements, and discoveries. Therefore, in a research group with extensive sample production and characterization with a large amount of data, a system that automatically reads data and displays the necessary, and of high interest, results should be of great interest.

In this paper we show a programming approach to support the community to stablish performance metrics for SC devices, with standard terms, equations, and units. We provide an overview of the supercapacitor characteristics and key parameters and discuss all the equations used for each analysis and the results generated by the SCAA to show how automating this process may make uniform and accelerate data analysis with fast interpretation and understanding of the results.

In this version, our program aims for simplicity, where the user inputs the data and a few specific parameters of the samples and characterization before running the analysis. The SCAA program presents the equations to precisely calculate the key parameters from the measurement and the specified device and conditions. The program generates many outputs - better described later – in the form of graphs, along with . txt files in case the user needs further manipulation.

## 2. Methods

Electrochemical characterizations were performed in symmetric all-solid SCs based on PEDOT:PSS, prepared by our research group, in a two-electrode system using a potentiostat (AutoLab Metrohm, PGStat coupled with the FRA32 module). We performed cyclic voltammetry (CV) using scan rates of 10 to 200 $mV{\cdot}s^{-1}$; galvanostatic charge–discharge (GCD) measurements were performed with specific current range from 0.1 to 1.0 $A{\cdot}g^{-1}$. Both measurements were performed with the same potential window of 0.8 V and generated one data file for each scan rate/specific current step (Fig. S1). Cycle stability was performed by CV and GCD: 5000 CV cycles at a scan rate of 200 $mV{\cdot}s^{-1}$, and 5000 GCD cycles at 0.2 $A{\cdot}g^{-1}$. Electrochemical Impedance Spectroscopy (EIS) was performed using 2 electrodes method at the open circuit potential with an amplitude of 10 mV in a frequency range from 0.1 to $10^5$ Hz. The mass of both active electrodes was 1.2 mg deposited over an area of 0.64 $cm^2$, and a total volume of 0.000512 $cm^3$. The electrolyte was 1.2 M $H_3PO_4$-PVA gel-electrolyte.

### 2.1. Program, interfaces, inputs and outputs

The software was developed using the programming language Python (version 3.8.5). Understanding properly the data researchers hold is important to use the appropriate equations and graphs to obtain individual and important SC parameters. From the CV data, the files are separated by different potential scan rates for which the measurement was performed, and each file presents only two columns: Voltage and Current. From that point on, the software performs the reading of all files and places them together in a single file (Fig. S1). The same process occurs for GCD data, which initially also presents many files corresponding to different specific currents to charge–discharge the device. Once this initial organization process is complete, the program treats the data to proper units or normalization (that is, F to $F{\cdot}g^{-1}$, $F{\cdot}cm^{-2}$, and $F{\cdot}cm^{-3}$). The outputs from the SCAA program are Ragone plot, CV plotting (*I vs V*), capacitance (*C*), energy (*E*), and power (*P*) *vs* potential scan rate, while the GCD outputs are *C*, *E*, *P vs* specific current, GCD graph (*V vs t*),

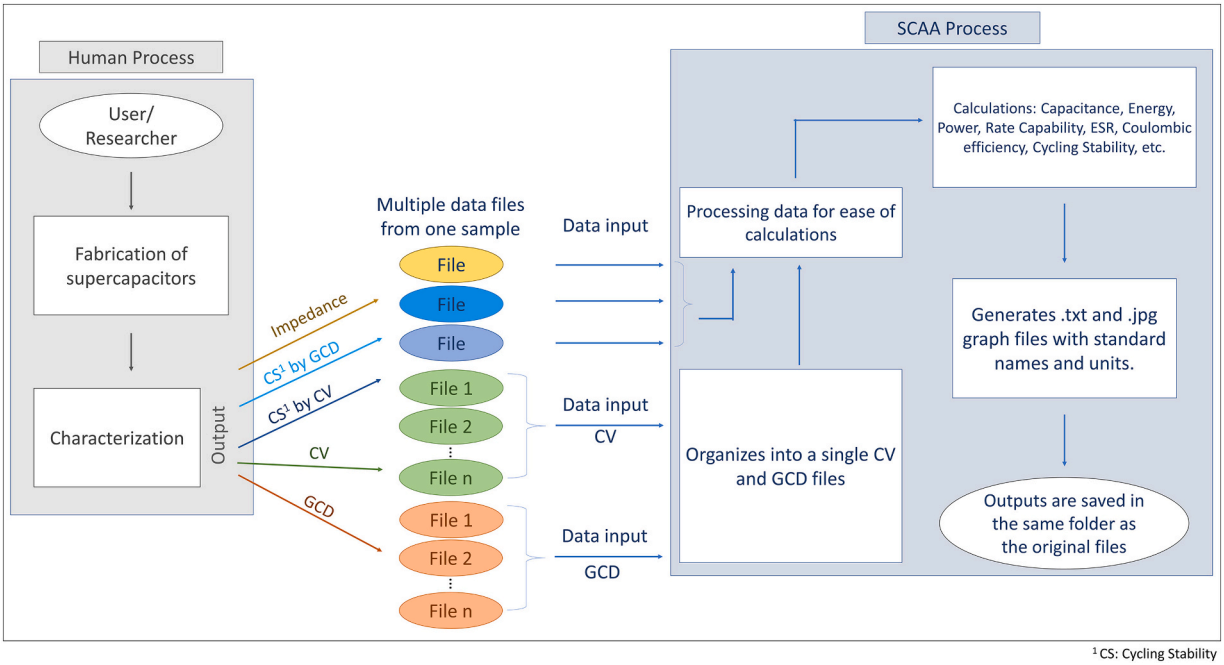


**Fig. 1.** Simplified flowchart representation of the SCAA processes after sample production, electrochemical characterization, and data collection to feed the SCAA program.

**Inputs required from each measurement (Columns, values and units)**

| CV | GCD | EIS | CS[1] by CV | CS[1] by GCD |
|---|---|---|---|---|
| **2 columns** from each scan rate (V/s): I (A), V (V) | **4 columns** from each specific current (A/g): time for charging (s) and respective V (V); time for discharging and respective V (V) | **5 columns:** f (Hz); Phase (°); Abs Z (Ω); Real Z (Ω); Imag. Z (Ω) | **3 columns:** Cycle, I (A), V (V) | **4 columns[2]** time for charging (s) and respective V (V); time for discharging and respective V (V) |

**Output of each analysis (.txt and/or graph)**

| Output (units) | CV | GCD | EIS | CS[1] by CV | CS[1] by GCD |
|---|---|---|---|---|---|
| **C** (F/g, F/cm²)* | ✓ | ✓ | ✓ | ✓ | ✓ |
| **E** (Wh/kg, Wh/cm²)* | ✓ | ✓ | | ✓ | ✓ |
| **P** (W/kg, W/cm²)* | ✓ | ✓ | | ✓ | ✓ |
| **Ragone Plot** | ✓ | ✓ | | | |
| **ESR** (Ω) | | ✓ | ✓ | | ✓ |
| **$V_{DROP}$** (V) | | ✓ | | | ✓ |
| **CE** (%) | | ✓ | | | ✓ |
| **EF** (%) | | ✓ | | | ✓ |
| **VE** (%) | | ✓ | | | |
| **Cycling Stability** | | | | ✓ | ✓ |

[1] CS: Cycling Stability
[2] Repeated n cycles
* and volumetric units

**Fig. 2.** Standard requirement for input data; and SCs key properties generated from each analysis by the SCAA program. Further information about the input files is shown in Figs. S1 and S2 from the Supplementary Information.

as well as parameters of equivalent series resistance (*ESR*), coulombic, energy and voltage efficiencies (*CE*, *EE*, and *VE*, respectively).

From data of cycling stability obtained from thousands of CV and GCD cycles, the main outputs are CV (*I vs V* over *n* cycles) or GCD (*V vs t*) and the respective stability over cycles, dropping from 100 % at cycle number 1 to smaller values after *n* cycles.

The EIS data are organized for plotting the main graphs: Bode plots, Nyquist plots, capacitance, and time constant *vs* Frequency. From the Nyquist plot it is obtained the ESR by taking the lowest value from the Z' data (Real Impedance), taken at the highest frequencies, while the specific capacitance and time constant are presented ahead.

The whole process from the sample fabrication to final data analysis

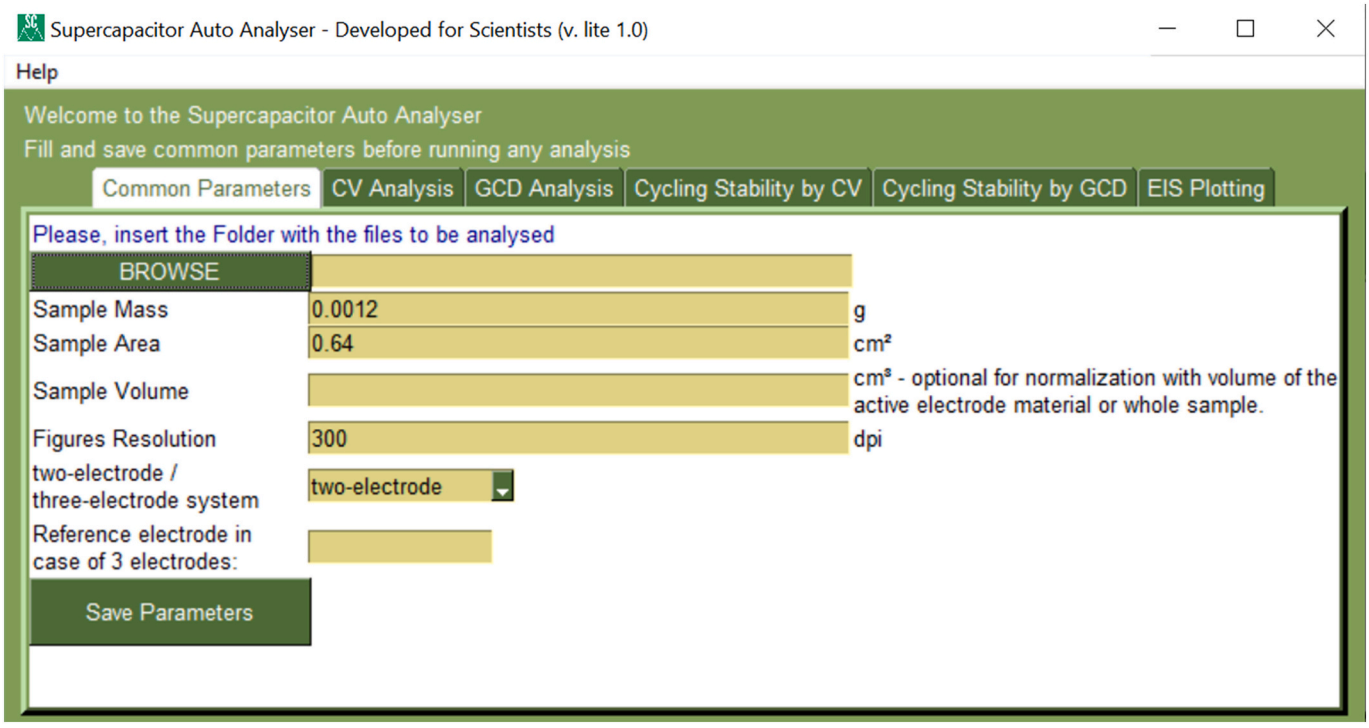


**Fig. 3.** Graphical User Interface (GUI) of the SCAA program for folder and file inputs and few parameters for each analysis. Images of the other tabs and parameters required are shown in the SI.

is simplified and schematized as shown in Fig. 1.

Fig. 2 summarizes the standards required for the input data and the key parameters generated by each analysis. GCD is a crucial measurement that is responsible for a great part of the results, either by single GCD measurements or by cycling stability. Further information about the input files is available in the Supplementary Materials, Figs. S1 and S2, and additional document with instructions for data acquisition using the software Nova 2.1.5 from the AutoLab is also available.

Fig. 3 presents the SCAA's graphical user interface (GUI) where the user should input the data files and some common parameters such as: the mass, area, and volume of the sample, to individually analyse in the respective tab, according to the file input. This GUI was made using the PySimpleGUI library from Python, and the SCAA program turned into an executable file, so the users would not need programming skills or Python to run the analysis.

General equations, units, and names used in the algorithm (and interface) are presented in the next sections. The equations were obtained from the supercapacitor literature and mainly from Noori et al.' review [16].

### 2.2. CV data analysis

The Eq. (1) for capacitance $C_x$ (in units of F·g$^{-1}$, F·cm$^{-2}$ or F·cm$^{-3}$) considers the capacitive potential interval $\Delta V$ (V), the potential scan rate $\nu$ in (V·s$^{-1}$), the whole device or electrodes mass (g), their area (cm$^2$) or volume (cm$^3$) as $x$, and the integration of $idV$ under the reverse part of CV (*i.e.* discharge scan, from $V_f = 0.8$ V to $V_i = 0$) to obtain the voltametric charge (in units of A·V)

$$C_x = \frac{1}{\nu\, x \Delta V} \int_{V_f}^{0} i\, dV \tag{1}$$

It is important to note the difference of true area-normalized capacitance and geometric area normalized capacitance, where the first is more inconsistent and complicated to obtain due to equipment variability in surface area measurements, especially in the case of porous active materials [16], whereas the geometric area normalized capacitance is the ratio of the capacitance to the simple geometric surface area of electrode exposed to the electrolyte. Thus, the user must pay attention to the sample area input that will result in the respective normalized capacitance.

The energy is taken from the equation $E_x = \frac{(C_x\, \Delta V^2)}{2}$, $E_{mass}$ is adjusted to h and kg resulting in units of Wh·kg$^{-1}$, while $E_{area/volume}$ takes area (cm$^2$) or volume (cm$^3$) and is adjusted to h and presents units of Wh·cm$^{-2}$ or Wh·cm$^{-3}$.

$$E_{mass} = \frac{C_{mass} \Delta V^2}{7.2} \text{ or } \quad E_{area/volume} = \frac{C_{area/volume} \Delta V^2}{7200} \tag{2}$$

The Eq. (3) for the power $P_x$ is adjusted to h, resulting in units of either W·kg$^{-1}$, W·cm$^{-2}$ or W·cm$^{-3}$.

$$P_x = \frac{E_x\, \nu\, 3600}{\Delta V} \tag{3}$$

Cycling stability $CS_{CV}$ (%) normally obtained from several thousand GCD cycles, in the SCAA it is also obtained for several thousand ($n$) CV cycles. The result is calculated and shown considering the percent retention of capacity from the first cycle ($C_{n=1} = 100$ %) through the $n$ CV cycles.

$$CS_{CV}(\%) = \frac{C_n}{C_{n=1}} \times 100 \tag{4}$$

As this measurement may be destructive to the sample, we recommend that the user give priority for Cycling Stability by GCD that is more reliable and produces more key parameters along the $n$ cycles.

### 2.3. GCD data analysis

For the capacitance, or $q/\Delta V$ value, which is more correct for hybrid systems, the calculation from GCD data integrates the discharge during the discharge time ($t_d$), as shown in Eq. (5). The equation is composed of the amount of storage electric charge $q$ in Coulomb (C), current ($i$), potential window ($\Delta V$), drop potential ($V_{Drop}$), and $x$ for mass (g), area (cm$^2$) or volume (cm$^3$). This general equation, although more complex, considers any shape that the discharge curve may present.

$$\frac{q}{V} = \frac{2i}{x\left(\Delta V - V_{Drop}\right)^2} \int_0^{t_d} \Delta V\, dt \tag{5}$$

Notice that the SCAA uses a normalized specific current (A·g$^{-1}$) from the GCD input data (see Fig. 2), then $x$ is removed from the equation within the program. For area and volume normalization the SCAA multiplies the equation by the mass provided by the user and divides by the area or volume also input by the user.

The energy takes the integration of the discharge curve times the normalized specific current (A·g$^{-1}$) and is adjusted to kg and h for $E_{mass}$ (Wh·kg$^{-1}$), and just to h for $E_{area/volume}$ (Wh·cm$^{-2}$ or Wh·cm$^{-3}$).

$$E_{mass} = \frac{i}{3.6} \int_0^{t_d} \Delta V\, dt \text{ or } \quad E_{area\ or\ volume} = \frac{i}{3600} \int_0^{t_d} \Delta V\, dt \tag{6}$$

The equation for power $P_x$ receives the $E_x$ and divides by $t_d$ converted from s to h and is given in units of W·kg$^{-1}$, W·cm$^{-2}$ or W·cm$^{-3}$.

$$P_x = \frac{E_x\, 3600}{t_d} \tag{7}$$

The Equivalent Series Resistance (ESR) in Eq. (8) takes the $V_{drop}$ from the difference between the highest charge potential and the highest discharge potential, right after starting the discharge process. ESR (Ω) accounts for the sum of resistances of the electrode, as well as between electrode and current collector, and bulk electrolyte.

$$ESR = \frac{V_{Drop}}{2i} \tag{8}$$

The Coulombic efficiency ($CE$) takes the ratio of charges extracted against charges inserted in the SC. As the GCD occurs at constant current for charging or discharging, the CE is simplified as shown in the right-hand side of Eq. (9):

$$CE(\%) = \frac{\Delta q_d}{\Delta q_c} \times 100 = \frac{\int_0^{t_d} i_d dt}{\int_0^{t_c} i_c dt} \times 100 = \frac{t_d}{t_c} \times 100 \tag{9}$$

where $q_d$ is the discharged electrical charge (C) from the SC, $q_c$ is the charged electrical charge (C) to the SC, $t_c$ and $t_d$ are the charging and discharging times, respectively.

Similarly, energy efficiency ($EE$) takes the ratio between energy discharged ($E_d$) and charged ($E_c$), while voltage efficiency (VE) takes the ratio between $EE$ and $CE$. Both equations are presented in Eqs. (10) and (11), respectively.

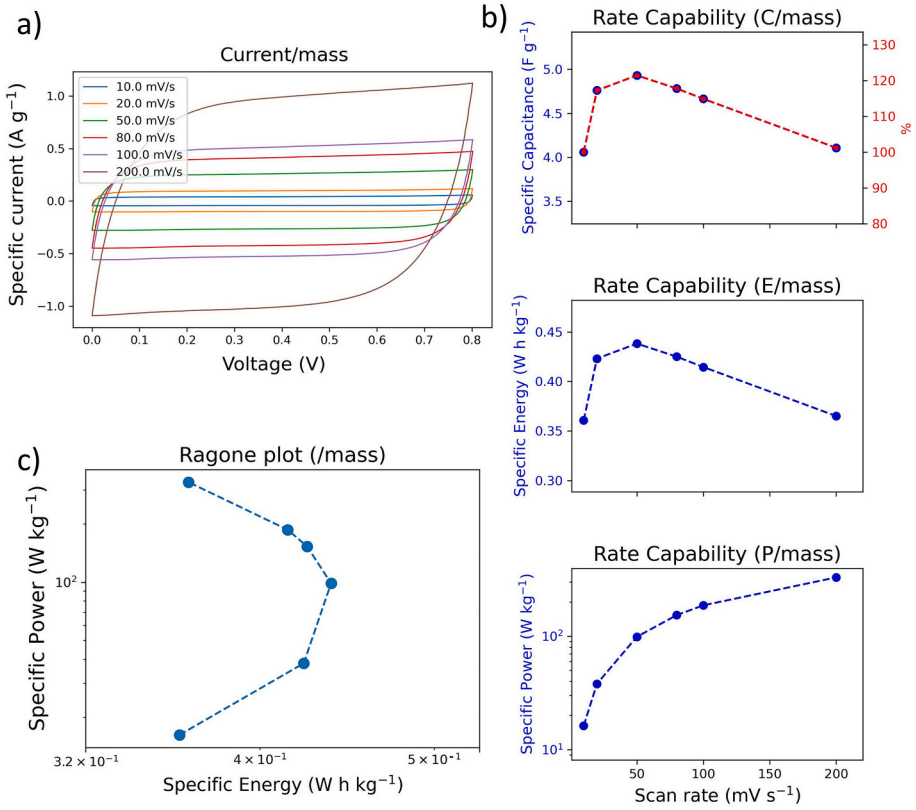


**Fig. 4.** Graphs generated from the CV data analysis by the SCAA. a) CV graph for different scan rates, b) rate capability of specific capacitance, energy and power. C) Ragone plot, with specific energy *vs* specific power. Here, it is only shown specific units (per unit of mass) for better convenience. Fig. S3 presents the other normalizations (area and volume) generated by the SCAA.

$$EE(\%) = \frac{E_d}{E_c} \times 100 \tag{10}$$

$$VE(\%) = \frac{EE}{CE} \times 100 \tag{11}$$

The most appropriate form of Cycling stability ($CS_{GCD}$) obtained from several thousand GCD cycles is calculated and shown as for CV ones, using Eq. (4), and considers the percent retention of capacity from the first cycle ($C_{n=1} = 100$ %) through the $n$ GCD cycles.

$$CS_{GCD}(\%) = \frac{C_n}{C_{n=1}} \times 100 \tag{12}$$

### 2.4. EIS data analysis

Previous CV and GCD analysis retrieve integral capacitance, while EIS brings the differential capacitance. Eq. (13) presents the differential capacitance ($C$) from the Imaginary Impedance ($Z_{im}$) and frequency ($f$) provided by the EIS data and normalized to specific capacitance using the sample mass ($m$).

$$C_{mass} = \frac{1}{(2\,\pi\,f\,|Z_{im}|)\,m} \tag{13}$$

The time constant ($\tau_f$) expressed by Eq. (14) takes the real impedance ($Z_{real}$) and capacitance (in F):

$$\tau_f = RC = Z_{real}\,\frac{1}{(2\,\pi\,f\,|Z_{im}|)} \tag{14}$$

## 3. Results

From the CV data, the SCAA returns the following graphs presented in Fig. 4: voltammogram (Fig. 4(a)), useful for visual differentiation of the characteristic type of device, a capacitor, or battery-type. This experiment provides quantitative and qualitative data related to the electrochemical processes that occur in the electrode material [21,22]. The analysis also provides values of capacitance, potential window, energy, and power, as well as their rate capabilities (Fig. 4(b)), and Ragone plot (Fig. 4(c)).

Both energy and power are essential parameters to understand the performance of electrochemical energy storage devices (EESD), and they are related and shown in the Ragone plot, which is incredibly important for performance evaluation of different EESD. By either form, specific (per unit of mass) or density (per unit of area) or volumetric (per unit of volume), they show the energy stored in an EESD and the power this EESD can deliver.

GCD data analysed by the program returns the graphs presented in Figs. 5 and 6, as well as their respective .txt files. It is important to observe that although CV and GCD operate on fundamentally different mechanisms, the metrics derived from their analysis should present similar values when low scan rate ($\nu$) and specific current ($i$) are considered, respectively. GCD analysis is a better fit determining the capacitance, energy, and power.

Through the GCD data, it is possible to obtain the most important parameters of SCs such as capacitance, potential window, and equivalent series resistance, as well as inferring the values of time constant, energy and power, in addition to being used for cyclic stability tests. GCD also provides quantitative information on transport kinetics in SCs, electrochemical performance, and device efficiency. When analysed in a

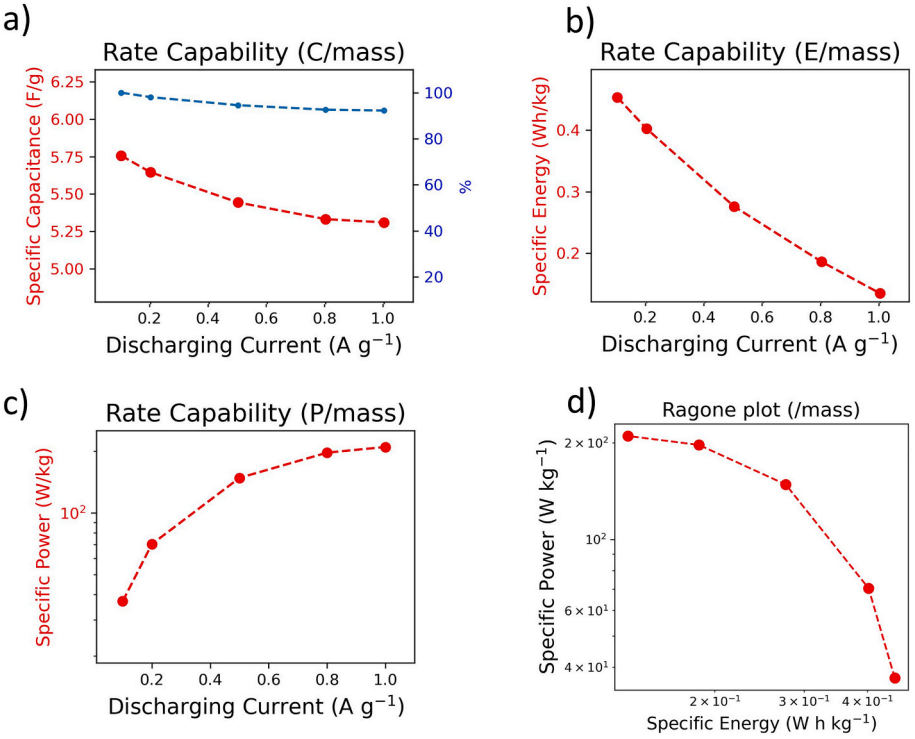


**Fig. 5.** Graphs generated as outputs of GCD data analysis. a) rate capability of specific capacitance, b) energy and c) power. d) Ragone plot, with specific energy *vs* specific power. Only units of sample mass for better convenience.

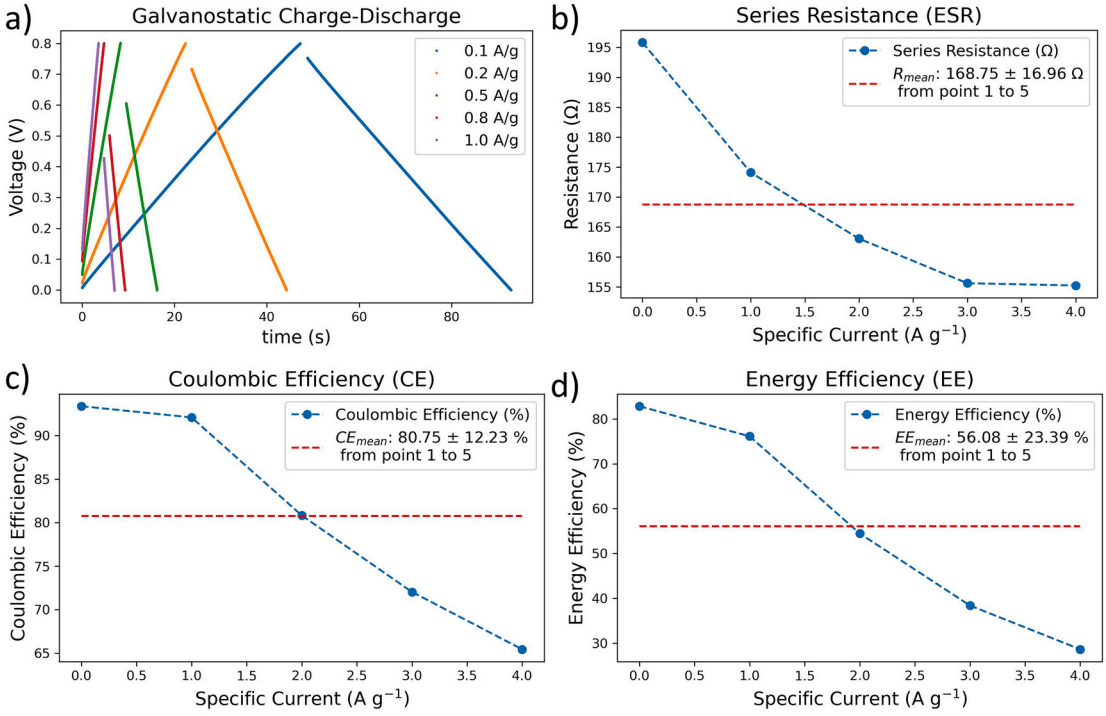


**Fig. 6.** Graphs generated as output of GCD data analysis. a) GCD curves for different specific charging/discharging currents. b) *ESR*, c) *CE*, and d) *EE versus* specific current.

three-electrode system, the reversibility, capacitance, and potential window of the active material can be obtained.

Rate capability, either by CV (Fig. 4) or GCD (Fig. 5), measures the conservation of capacitance/capacity as a function of $\nu$ (CV) or $i$ (GCD), where the capacitance usually reduces at increasing $\nu$ or $i$. High rate capability indicates higher accessibility of ions to most of the pores and surface area of the active electrode material, and a fast kinetics of electrode processes, such as fast ion/electron transport [23,24]. This parameter indicates that an improvement may be reached by controlling the pore size and the specific surface area of the active electrode material.

As suggested by Noori and collaborators [16], it is of fundamental importance to provide a more realistic picture of the EESD by showing the key parameters obtained by GCD normalized by mass, area, and volume of the active electrode material as well as of the whole package, which includes supporting components as current collectors, electrolytes, binders, separators, and casing. Although Fig. 5 only shows different parameters normalized to mass, the program provides all the normalizations - /area ($cm^2$), /volume ($cm^3$) – shown in Fig. S4 of the Supplementary Material.

Other graphs showing important parameters, such as charge−discharge time, *ESR*, *CE*, and *EE* are shown in Fig. 6. The program also calculates the mean value of each efficiency parameter. The *ESR* value represents the sum of the electrolyte resistance, the contact resistance between the electrode and the current collector and the resistance of the electrode itself. The *ESR* value restricts the speed at which a SC can start the loading or unloading process, which implies that higher *ESR* values provide lower SC's performance. Although the *ESR* calculated from GCD is not more precise than that one obtained from *EIS*, it is one of the generated parameters obtained and displayed to the user. *EE* is described as the ratio of electrical energy drawn out from a device to the electrical energy required to put the energy storage device back to the same state of charge. Further parameters are present in Fig. S5 of the Supplementary Material.

Cycling stability analysis results are shown in Fig. 7. Although this valuable measurement mainly obtained and reported by GCD, the SCAA also analyses the data obtained by CV for comparison. The user may run this measurement under different conditions, such as temperatures, humidity, deformation (in case of flexible or stretchable samples), potential windows and current, to understand the dependence of the cycle life based in those conditions [25,26]. As a standard protocol for consistent assessment of energy storage systems, SCs should present ~10,000 cycles, while the hybrid system has a lifetime of around 5000 cycles [27]. Fig. S6 and S7 of the Supplementary material presents more graphs related to both Cycling Stability tests, by CV and GCD, where GCD's presents the variations of *C*, *E*, *P*, *ESR*, and Efficiencies (*CE*, *EE*, and *VE*) along the *n* cycles.

This analysis helps the researcher to understand the possible degradations occurring in the active material induced by corrosion in the cell components, which decreases capacitance and increases ESR, as a prediction of how the SC will behave in real-world applications, where thousands of loading and unloading cycles will be performed.

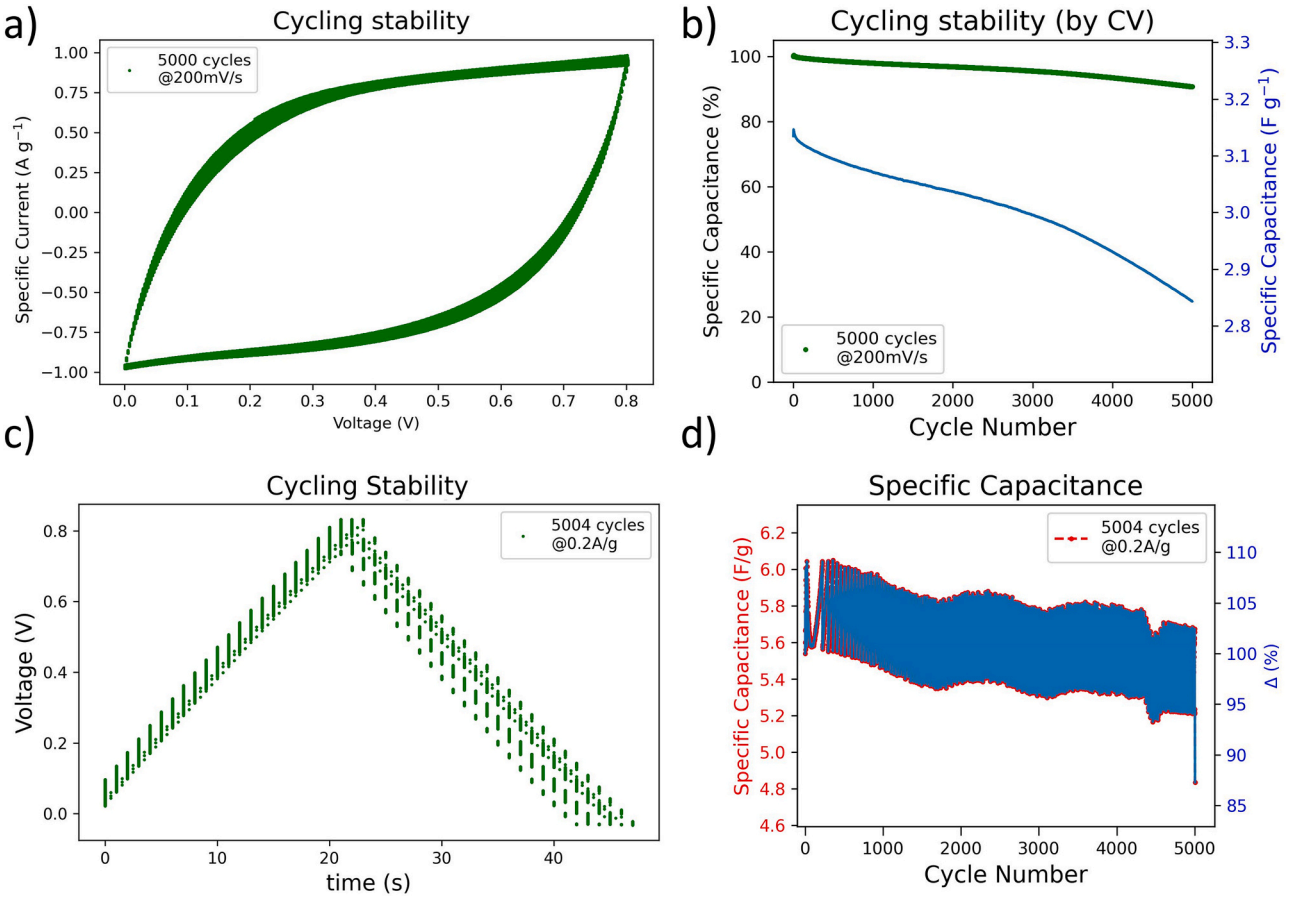


**Fig. 7.** Cycling stability curves by a-b) CV and c-d) GCD for *n* cycles. In this study, 5000 cycles were performed for both measurements.

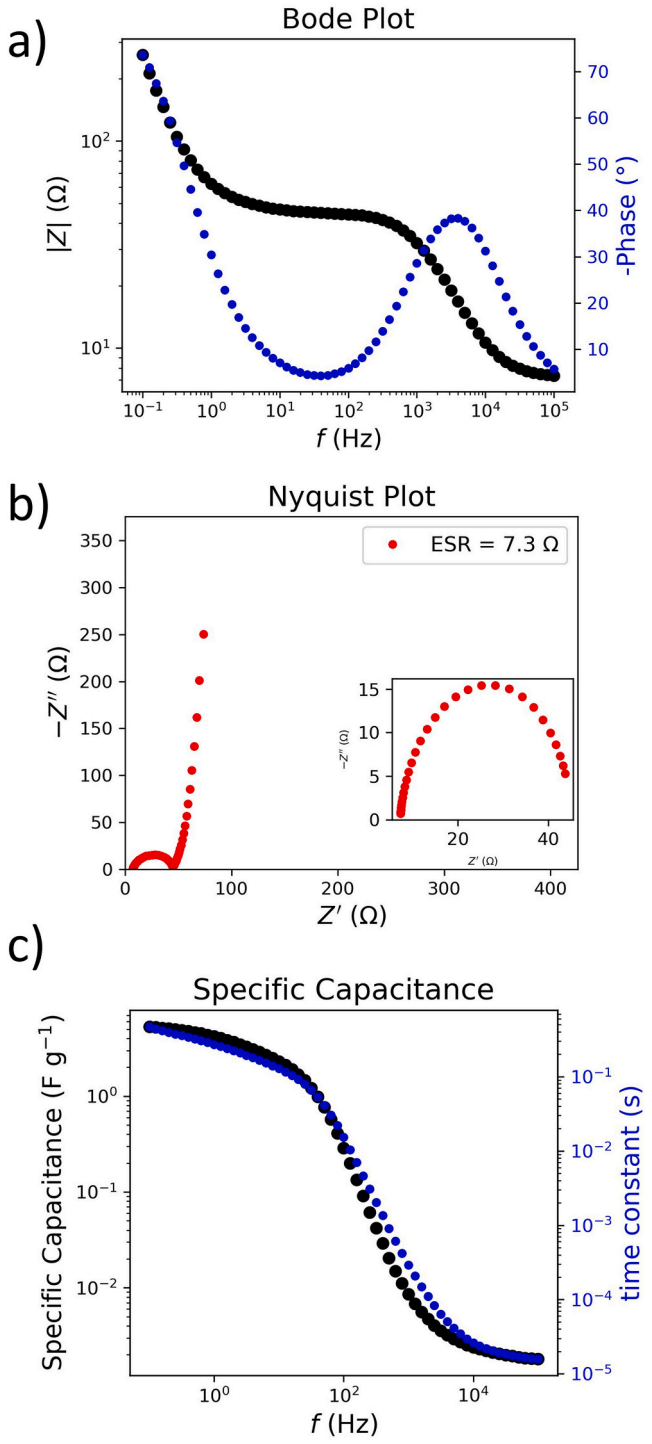


**Fig. 8.** Plotting of a) Bode and b) Nyquist plots from EIS data. c) Calculated specific capacitance and time constant. Areal and volumetric capacitance are also generated by the SCAA and are shown in the Fig. S8 of the Supplementary Material.

The powerful EIS can provide useful information through its common Nyquist and Bode plots [28,29]. Besides plotting these graphs, the SCAA does some further calculations (Eqs. (13) and (14)) to display the normalized specific (areal and volumetric) capacitance and time constant, both plotted *vs* frequency (Fig. 8). The ESR is also calculated and displayed together with the Nyquist plot.

## 4. Conclusions

In this work we presented a program to facilitate and help stablish performance metrics in the analysis of supercapacitor devices. The results were taken from the inputs of CV, GCD and EIS characterizations of symmetric SCs based on PEDOT:PSS. The Supercapacitor Auto Analyser (SCAA) performs a relevant contribution to data analysis of the properties of SCs, quickly showing the key parameters to help researchers not only improve their initial analysis but also keep standard units, nomenclature, and equations for calculations. In a few minutes as many as 50 normalized graphs are generated accordingly with the inputs provided by the users, displaying the necessary, and of high interest, key parameters of their devices. The present work can speed up research on supercapacitors through automation of data analysis, packed in a software shared with the community in the supplementary materials and website www.scaasoftware.com.

## CRediT authorship contribution statement

**Miguel H. Boratto:** Conceptualization, Methodology, Formal analysis, Software, Validation, Writing – original draft. **João V.M. Lima:** Resources, Investigation, Validation, Writing – original draft. **George G. Malliaras:** Supervision. **Carlos F.O. Graeff:** Supervision.

## Declaration of competing interest

The authors declare that they have no known competing financial interests or personal relationships that could have appeared to influence the work reported in this paper.

## Data availability

Data will be made available on request.

## Acknowledgements

This work was supported by FAPESP (Grants numbers 2013/07296-2, 2017/20809-0, 2020/04721-8, 2020/12356-8, 2021/03379-7).

## Appendix A. Supplementary data

Supplementary data to this article can be found online at https://doi.org/10.1016/j.est.2023.107095.

## References

[1] Y. Shao, M.F. El-Kady, J. Sun, Y. Li, Q. Zhang, M. Zhu, H. Wang, B. Dunn, R. B. Kaner, Design and mechanisms of asymmetric supercapacitors, Chem. Rev. 118 (2018) 9233–9280, https://doi.org/10.1021/acs.chemrev.8b00252.
[2] S. Huang, X. Zhu, S. Sarkar, Y. Zhao, Challenges and opportunities for supercapacitors, APL Mater. 7 (2019), 100901, https://doi.org/10.1063/1.5116146.
[3] P. Simon, Y. Gogotsi, Materials for electrochemical capacitors, Nat. Mater. 7 (2008) 845–854, https://doi.org/10.1038/nmat2297.
[4] D.G. Nocera, Living healthy on a dying planet, Chem.Soc.Rev. 38 (2009) 13–15, https://doi.org/10.1039/B820660K.
[5] J. Yan, Q. Wang, T. Wei, Z. Fan, Recent advances in design and fabrication of electrochemical supercapacitors with high energy densities, Adv. Energy Mater. 4 (2014), 1300816, https://doi.org/10.1002/aenm.201300816.
[6] A. González, E. Goikolea, J.A. Barrena, R. Mysyk, Review on supercapacitors: technologies and materials, Renew. Sust. Energ. Rev. 58 (2016) 1189–1206, https://doi.org/10.1016/j.rser.2015.12.249.
[7] Poonam, K. Sharma, A. Arora, S.K. Tripathi, Review of supercapacitors: Materials and devices, J. Energy Storage 21 (2019) 801–825, https://doi.org/10.1016/j.est.2019.01.010.
[8] A. Ehsani, M.K. Moftakhar, F. Karimi, Lignin-derived carbon as a high efficient active material for enhancing pseudocapacitance performance of p-type conductive polymer, J. Energy Storage 35 (2021), 102291, https://doi.org/10.1016/j.est.2021.102291.
[9] H.-L. Girard, H. Wang, A. d'Entremont, L. Pilon, Physical interpretation of cyclic voltammetry for hybrid pseudocapacitors, J. Phys. Chem. C 119 (2015) 11349–11361, https://doi.org/10.1021/acs.jpcc.5b00641.

[10] L. Zhang, X. Hu, Z. Wang, F. Sun, D.G. Dorrell, A review of supercapacitor modeling, estimation, and applications: a control/management perspective, Renew. Sust. Energ. Rev. 81 (2018) 1868–1878, https://doi.org/10.1016/j.rser.2017.05.283.
[11] P.E. Lokhande, U.S. Chavan, A. Pandey, Materials and fabrication methods for electrochemical supercapacitors: overview, Electrochem.Energy Rev. 3 (2020) 155–186, https://doi.org/10.1007/s41918-019-00057-z.
[12] A. Muzaffar, M.B. Ahamed, K. Deshmukh, J. Thirumalai, A review on recent advances in hybrid supercapacitors: design, fabrication and applications, Renew. Sust. Energ. Rev. 101 (2019) 123–145, https://doi.org/10.1016/j.rser.2018.10.026.
[13] L. Li, N. Zhang, M. Zhang, X. Zhang, Z. Zhang, Flexible Ti3C2Tx/PEDOT:PSS films with outstanding volumetric capacitance for asymmetric supercapacitors, Dalton Trans. 48 (2019) 1747–1756, https://doi.org/10.1039/C8DT04374D.
[14] L. Liu, P.-L. Taberna, B. Dunn, P. Simon, Future directions for electrochemical capacitors, ACS Energy Lett. 6 (2021) 4311–4316, https://doi.org/10.1021/acsenergylett.1c01981.
[15] A. Ehsani, H. Parsimehr, H. Nourmohammadi, R. Safari, S. Doostikhah, Environment-friendly electrodes using biopolymer chitosan/poly ortho aminophenol with enhanced electrochemical behavior for use in energy storage devices, Polym. Compos. 40 (2019) 4629–4637, https://doi.org/10.1002/pc.25330.
[16] A. Noori, M.F. El-Kady, M.S. Rahmanifar, R.B. Kaner, M.F. Mousavi, Towards establishing standard performance metrics for batteries, supercapacitors and beyond, Chem. Soc. Rev. 48 (2019) 1272–1341, https://doi.org/10.1039/C8CS00581H.
[17] T. Huang, X. Chu, S. Cai, Q. Yang, H. Chen, Y. Liu, K. Gopalsamy, Z. Xu, W. Gao, C. Gao, Tri-high designed graphene electrodes for long cycle-life supercapacitors with high mass loading, Energy Storage Mater. 17 (2019) 349–357, https://doi.org/10.1016/j.ensm.2018.07.001.
[18] J. Cao, Y. Wang, Y. Zhou, J.H. Ouyang, D. Jia, L. Guo, High voltage asymmetric supercapacitor based on MnO2 and graphene electrodes, J. Electroanal. Chem. 689 (2013) 201–206, https://doi.org/10.1016/j.jelechem.2012.10.024.
[19] S. Dai, Z. Liu, B. Zhao, J. Zeng, H. Hu, Q. Zhang, D. Chen, C. Qu, D. Dang, M. Liu, A high-performance supercapacitor electrode based on N-doped porous graphene, J. Power Sources 387 (2018) 43–48, https://doi.org/10.1016/j.jpowsour.2018.03.055.
[20] S.Y. Attia, S.G. Mohamed, Y.F. Barakat, H.H. Hassan, W. al Zoubi, Supercapacitor electrode materials: addressing challenges in mechanism and charge storage, Rev. Inorg. Chem. 42 (2022) 53–88, https://doi.org/10.1515/revic-2020-0022.
[21] H. Yang, T. Xiong, Z. Zhu, R. Xiao, X. Yao, Y. Huang, M.Sadeeq Balogun, Deciphering the lithium storage chemistry in flexible carbon fiber-based self-supportive electrodes, Carbon Energy 4 (2022) 820–832, https://doi.org/10.1002/cey2.173.
[22] G. Li, T. Ouyang, T. Xiong, Z. Jiang, D. Adekoya, Y. Wu, Y. Huang, M. Saqeed Balogun, All-carbon-frameworks enabled thick electrode with exceptional high-areal-capacity for Li-ion storage, Carbon 174 (2021) 1–9, https://doi.org/10.1016/j.carbon.2020.12.018.
[23] J. Yan, S. Li, B. Lan, Y. Wu, P.S. Lee, Rational design of nanostructured electrode materials toward multifunctional supercapacitors, Adv. Funct. Mater. 30 (2020), 1902564, https://doi.org/10.1002/adfm.201902564.
[24] L.M. da Silva, R. Cesar, C.M.R. Moreira, J.H.M. Santos, L.G. de Souza, B.M. Pires, R. Vicentini, W. Nunes, H. Zanin, Reviewing the fundamentals of supercapacitors and the difficulties involving the analysis of the electrochemical findings obtained for porous electrode materials, Energy Storage Mater. 27 (2020) 555–590, https://doi.org/10.1016/j.ensm.2019.12.015.
[25] P.K. Kahriz, H. Mahdavi, A. Ehsani, A.A. Heidari, M. Bigdeloo, Influence of synthesized functionalized reduced graphene oxide aerogel with 4,4′-methylenedianiline as reducing agent on electrochemical and pseudocapacitance performance of poly orthoaminophenol electroactive film, Electrochim. Acta 354 (2020), https://doi.org/10.1016/j.electacta.2020.136736.
[26] A. Ehsani, M. Bigdeloo, F. Assefi, M. Kiamehr, R. Alizadeh, Ternary nanocomposite of conductive polymer/chitosan biopolymer/metal organic framework: synthesis, characterization and electrochemical performance as effective electrode materials in pseudocapacitors, Inorg. Chem. Commun. 115 (2020), 107885, https://doi.org/10.1016/j.inoche.2020.107885.
[27] J. Ding, W. Hu, E. Paek, D. Mitlin, Review of hybrid ion capacitors: from aqueous to lithium to sodium, Chem. Rev. 118 (2018) 6457–6498, https://doi.org/10.1021/acs.chemrev.8b00116.
[28] X. Yao, C. Li, R. Xiao, J. Li, H. Yang, J. Deng, M.Sadeeq Balogun, Heterostructures stimulate electric-field to facilitate optimal Zn2+ intercalation in MoS2 cathode, Small 18 (2022), 2204534, https://doi.org/10.1002/smll.202204534.
[29] S. Zhou, P. Huang, T. Xiong, F. Yang, H. Yang, Y. Huang, D. Li, J. Deng, M. Sadeeq Balogun, Sub-thick electrodes with enhanced transport kinetics via in situ epitaxial heterogeneous interfaces for high areal-capacity lithium ion batteries, Small 17 (2021), 2100778, https://doi.org/10.1002/smll.202100778.